

## ON THE NATURE OF DARK EXTREME ULTRAVIOLET STRUCTURES SEEN BY *SOHO*/EIT AND *TRACE*

U. ANZER

Max-Planck-Institut für Astrophysik, Karl-Schwarzschildstrasse 1, D-85740 Garching, Germany

AND

P. HEINZEL

Astronomical Institute, Academy of Sciences of the Czech Republic, 25165 Ondřejov, Czech Republic

Received 2004 August 17; accepted 2004 November 28

### ABSTRACT

Spectral lines in the extreme ultraviolet (EUV) observed on the Sun can originate either from the hot corona or the cooler chromosphere to corona transition region. In the present paper we concentrate on coronal lines and in particular on iron lines at 171, 195, and 284 Å, which have been frequently observed by the *Solar and Heliospheric Observatory* (*SOHO*)/Extreme Ultraviolet Imaging Telescope (EIT) and the *Transition Region and Coronal Explorer* (*TRACE*). The intensity of these lines emitted by the corona can be reduced by the presence of a cool gas, e.g., by prominence-like material, located in the corona. There are two mechanisms that can lead to a reduction of the line intensity: *absorption* and *volume blocking*. That part of the coronal radiation that comes from behind the cool gas can be partially absorbed. The main absorbers for the iron lines studied here are neutral hydrogen and neutral plus singly ionized helium. In this paper we calculate the optical thickness of their resonance continua at the wavelength positions of iron lines and compare it with that in the H $\alpha$  line center. The comparison of the derived values shows that they are quite similar. The second effect is due to the fact that cool structures in the corona do not emit any radiation in the EUV lines, which gives rise to an additional reduction of the observed intensity as compared with the surrounding corona—we have termed this “volume blocking.” We further describe in this paper how these two effects can be used in a new way of performing prominence diagnostics. Our results are also applicable to other coronal lines detected by, e.g., the *SOHO* CDS or SUMER instruments.

*Subject headings:* Sun: corona — Sun: UV radiation

### 1. INTRODUCTION

Solar prominences and prominence-like structures (loops, surges, arch-filament systems, etc.) can be observed both on the disk and above the solar limb; when prominences are seen on the disk they are usually called filaments. Prominences are clearly visible in the H $\alpha$  line of neutral hydrogen. But with the recent generation of satellites they are now also observed in the extreme ultraviolet (EUV). Both transition region lines and coronal lines have been studied in this context. New particularly interesting observations come from the Extreme Ultraviolet Imaging Telescope (EIT) on board the *Solar and Heliospheric Observatory* (*SOHO*) and from the *Transition Region and Coronal Explorer* (*TRACE*). These instruments observe, among others, the iron lines of Fe IX at 171 Å, of Fe XII at 195 Å, and of Fe XV at 284 Å. The formation temperatures of these coronal lines lie at 1.3, 1.6, and 2.0  $\times 10^6$  K, respectively. In these lines cool structures are always dark, even when seen on the limb against the bright corona. EIT observations also include the transition-region line of He II at 304 Å, corresponding to a temperature of about 50,000 K. This helium line is particularly useful, because it allows the determination of the location of any prominence, both on the disk and on the limb. In addition to the EIT and *TRACE* iron lines, some other coronal EUV lines have been observed by the CDS and SUMER instruments on *SOHO*. There are many nice examples of such dark EUV structures observed by EIT, *TRACE*, or CDS, including illustrative movies. As one example, in Figure 1 we show the case of a filament-prominence configuration seen at a wavelength of 195 Å, which extends from the solar disk into the corona above the limb.

The quantitative analysis was performed in some recent papers (see Kucera et al. 1998, Chiuderi Drago et al. 2001, Heinzel

et al. 2001, Mein et al. 2001, Engvold et al. 2001, or Schmieder et al. 2004). Radiation of all EUV lines that lie below the head of the hydrogen Lyman continuum at 912 Å can be absorbed by neutral hydrogen, which is abundant in cool prominence structures (Schmahl & Orrall 1979). For even shorter wavelengths additional absorption by neutral helium can occur (below 504 Å), and for very short wavelengths (below 228 Å) singly ionized helium will also contribute under specific conditions. In the present paper we study all these absorption mechanisms in detail. Moreover, if the line emission comes from extended regions, as is the case for hot coronal lines, then volume blocking can also be a very important mechanism for the reduction of the line intensity. This point has been discussed previously by Heinzel et al. (2003) and in more detail by Schwartz et al. (2004).

In § 2 we describe the basic concepts of our modeling. Section 3 gives the results of our non-LTE radiative transfer calculations, which determine the relation between the optical thickness in H $\alpha$ ,  $\tau_{\text{H}\alpha}$ , and that at the head of the hydrogen Lyman continuum,  $\tau_{912}$ . In § 4 we evaluate the total absorption of the EUV lines in a cool plasma containing some fraction of neutral hydrogen and also neutral and singly ionized helium. Section 5 describes the volume blocking mechanism for prominences and filaments. Sections 6 and 7 summarize the results for prominences on the limb and for filaments on the disk, respectively. In § 8 we give a short outline of *extended EUV filaments*, and § 9 contains the conclusions.

### 2. BASIC ASPECTS

All cool structures (typically below 20,000 K) that extend into the hot solar corona can have essentially two effects on the radiation observed in the coronal EUV lines. If the lines

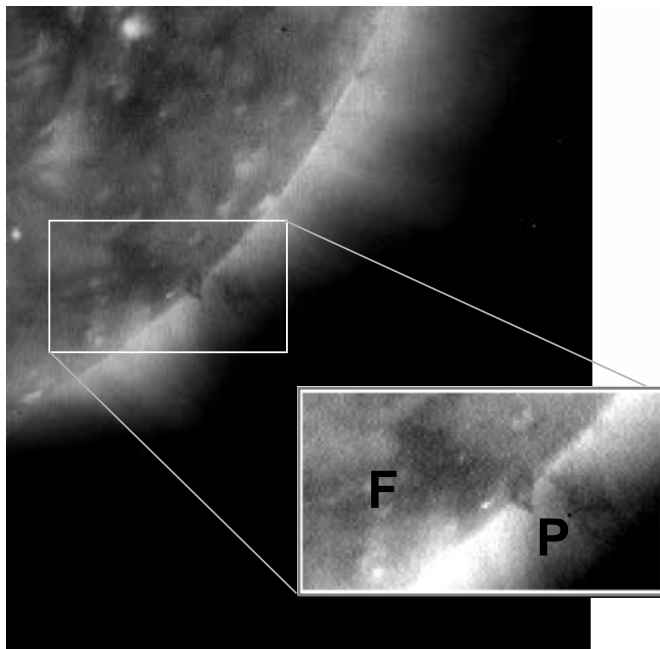


FIG. 1.—Example of dark EUV structures as observed by *SOHO*/EIT at a wavelength of 195 Å on 1997 July 4 at 07:12:30 UT. In this case a filament F is crossing the solar limb, and part of it is seen as a prominence P above the limb. Note also the iron-line corona at 195 Å with its radially decreasing brightness.

considered have wavelengths below 912 Å, then the radiation is subjected to absorption by hydrogen and helium resonance continua as it passes through the cool material. The second effect that can be present is volume blocking by cool material. In the case that the cool structures are sufficiently extended along the line of sight the part of the coronal volume occupied by cool plasma does not contribute to the emission in coronal lines, and therefore the total radiative output is correspondingly reduced compared with the neighboring corona. This latter effect can be dominant under many circumstances, as we will demonstrate later. In the present investigation we discuss both aspects, but the main emphasis is on absorption. For the different iron lines observed by EIT and *TRACE* the values of the continuum optical thickness at the wavelengths of the lines are different. However, they can be directly related to the value of  $\tau_{912}$  at the head of the hydrogen Lyman continuum. In addition, we want to compare the  $\tau$  values derived for particular EUV lines with those obtained from  $H\alpha$  observations. In order to do this we first have to establish a relation between  $\tau_{H\alpha}$  and  $\tau_{912}$  for different sets of prominence and filament models—this is based on a detailed non-LTE modeling described below. Once we have derived this relation, the values of  $\tau_{912}$  are used as the *unique reference values*. By adopting such a procedure one can directly compare the observed  $H\alpha$  structures with dark features that are seen in the EIT and *TRACE* iron line images.

### 3. DEPENDENCE OF $\tau_{912}$ ON $\tau_{H\alpha}$

The relation between the optical thickness at the hydrogen Lyman continuum head and that at the  $H\alpha$  line center can only be found by detailed non-LTE radiative transfer calculations. Heinzel et al. (2001) presented such a relation for the case of cool structures observed against the disk (such as filaments). They used a large grid of simple isobaric and isothermal models and showed that the relation between both opacities depends mainly on the temperature. The main result of their study was that for structures that become invisible in the  $H\alpha$  line ( $\tau_{H\alpha} < 0.1$ ),

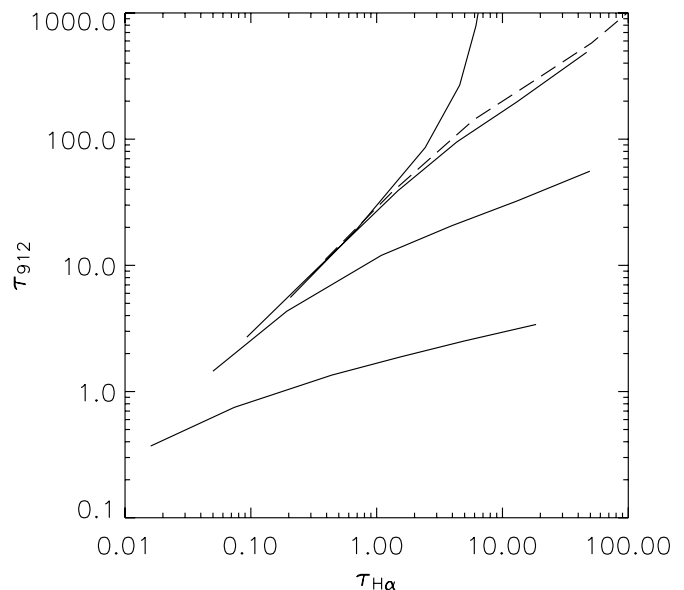


FIG. 2.—Correlation between the optical thickness at the head of the hydrogen Lyman continuum and that at the  $H\alpha$  line center for a grid of filament models described in the text. Here the four solid lines correspond (top to bottom) to the four filament temperatures of  $T = 6000, 8000, 10,000,$  and  $15,000$  K. These models have been computed for a geometrical thickness of 5000 km. The dashed line shows models with  $T = 8000$  K and with a thickness of 20,000 km.

the optical thickness at the hydrogen Lyman continuum head is still large enough for the cool structure to be visible because of the absorption of EUV line radiation by the continuum. The models used by Heinzel et al. (2001) have been originally computed for other purposes for which the assumption of complete frequency redistribution in Lyman lines was adequate. However, to obtain more precise and reliable correlations, one has to compute the opacities using the partial frequency redistribution. We did this kind of non-LTE modeling for purposes of this paper, and our results are shown in Figure 2. We again used the filament-like models, which are represented by a one-dimensional horizontal slab irradiated from below by the solar atmosphere (for technical details, see Heinzel et al. 1997). We consider four temperatures,  $T = 6000, 8000, 10,000,$  and  $15,000$  K, a micro-turbulent velocity of  $5 \text{ km s}^{-1}$ , and a unique geometrical thickness of the slab  $D = 5000$  km. Then different values of  $\tau$  were obtained by varying the gas pressure from 0.01 to 0.5 dyn  $\text{cm}^{-2}$ . To see the sensitivity of our correlations to  $D$ , we add one model at  $T = 8000$  K, having  $D = 20,000$  km. We see that the resulting curve differs only slightly from that for  $D = 5000$  km (the actual values of  $\tau_{912}$  and  $\tau_{H\alpha}$  are of course larger for larger  $D$ , but their ratio is almost independent of  $D$ ).

The fact that we prescribe  $D$ ,  $T$ , and  $p$  does not imply that we can obtain the densities analytically because the ionization degree depends in a complex manner on the radiative transfer. In our non-LTE calculations the hydrogen atom was taken as a 12-level model with continuum, and the partial frequency redistribution was used for the Lyman lines  $L\alpha$  and  $L\beta$ . The height above the photosphere at which the incident solar radiation was evaluated was taken as 10,000 km. This incident radiation plays an important role in the ionization structure of the filament. Let us also mention that the use of the partial frequency redistribution in this modeling lowers the curves for individual temperatures by about a factor of 3 as compared with those previously obtained with the complete frequency redistribution (compare with Fig. 2 in Heinzel et al. 2001).

For prominences on the limb, one has to use the identical non-LTE procedure but now applied to one-dimensional vertical slabs, standing perpendicularly to the solar surface and irradiated symmetrically from both sides. The same grid of models as we used for filaments leads to opacity correlations almost identical to those shown in Figure 2, and thus one can also use the curves from Figure 2 for prominences. A relevant grid of computed prominence models can be found in Gouttebroze et al. (1993). Small differences between the results for filaments and prominences are mainly due to a somewhat different irradiation of the one-dimensional slabs.

As already discussed by Heinzel et al. (2001), the results shown in Figure 2 have important consequences for dark structures seen against the solar disk. If a structure (e.g., filament) is clearly visible in the  $H\alpha$  line, one has  $\tau_{H\alpha} > 0.1$ . Then  $\tau_{912}$  is rather large, and the structure is capable of absorbing the EUV line radiation by hydrogen Lyman continuum. For  $\tau_{H\alpha} < 0.1$  the structure is no longer visible in  $H\alpha$ , but the Lyman continuum at 912 Å is still optically thick so that we can see extended EUV filaments identified in Heinzel et al. (2001) and Schmieder et al. (2003). However, the continuum absorption strongly decreases with decreasing wavelength, and in the far-EUV, at the position of EIT and *TRACE* iron lines, the resonance hydrogen and helium continua can be optically thin, as we demonstrate in the following section.

Finally, let us mention that  $\tau_{H\alpha}$  is directly related to the integrated prominence  $H\alpha$  intensity via the correlation derived by Heinzel et al. (1994; see their Fig. 5). This correlation is only weakly sensitive to temperature. To determine  $\tau_{H\alpha}$  for structures seen on the disk (such as filaments), one should apply the so-called cloud-model method, as discussed by, e.g., Mein et al. (2001).

#### 4. ABSORPTION OF IRON LINE RADIATION

##### 4.1. Basic Relations

The radiation of iron lines at 171, 195, and 284 Å observed with EIT and *TRACE* can be absorbed by intervening cool gas located in the corona. For wavelengths below 912 Å the absorption occurs by neutral hydrogen (Lyman continuum absorption); for  $\lambda < 504$  Å there is absorption by neutral helium, and for  $\lambda < 228$  Å also by singly ionized helium.

The total optical thickness of these continua at the wavelength position of the iron lines is given by

$$\tau = \sigma_H N_{H I} + \sigma_{He I} N_{He I} + \sigma_{He II} N_{He II}, \quad (1)$$

where  $N_{H I}$  is the total column density (i.e., density integrated along the line of sight) of neutral hydrogen, and  $N_{He I}$  and  $N_{He II}$  are those of neutral and singly ionized helium, respectively. The  $\sigma$ -values are the respective photoionization cross sections, which depend only on wavelength. Now, we define mean values for the ionization degrees of hydrogen and helium by

$$i = \frac{N_p}{N_H}, \quad (2)$$

where  $N_p$  and  $N_H$  are, respectively, the proton and total hydrogen column density, and

$$j_1 = \frac{N_{He II}}{N_{He}} \quad (3)$$

is the ionization degree of singly ionized helium and

$$j_2 = \frac{N_{He III}}{N_{He}} \quad (4)$$

TABLE 1  
FITTING COEFFICIENTS FOR He I CROSS SECTION

$i$	$c_i$
0.....	$-2.953607 \times 10^1$
1.....	$+7.083061 \times 10^1$
2.....	$+8.678646 \times 10^{-1}$
3.....	$-1.221932 \times 10^{-1}$
4.....	$+4.052997 \times 10^{-2}$
5.....	$+1.317109 \times 10^{-1}$
6.....	$-2.953607 \times 10^{-2}$
7.....	$+2.500933 \times 10^{-3}$

is the ionization degree of helium in its second ionization state. For total hydrogen and helium density we have, respectively,  $N_H = N_{H I} + N_p$  and  $N_{He} = N_{He I} + N_{He II} + N_{He III}$ . The abundance of helium relative to hydrogen is

$$r_{He} = \frac{N_{He}}{N_H}, \quad (5)$$

and in this study we take the value  $r_{He} = 0.1$ . Since we are dealing here with column densities, the quantities  $i$ ,  $j_1$ , and  $j_2$  all represent mean values of the ionization degrees. But in reality the local values of the ionization degrees can vary within each filament (see, e.g., Anzer & Heinzel [1999] and Labrosse & Gouttebroze [2004]). This effect has to be taken properly into account.

Using the above expressions, we can finally write

$$\tau = N_H \{ (1 - i) \sigma_H + r_{He} [ (1 - j_1 - j_2) \sigma_{He I} + j_1 \sigma_{He II} ] \}. \quad (6)$$

The photoionization cross sections are given by (see Mihalas 1978)

$$\sigma_H(\lambda) = \sigma_0 g_H(\lambda) (\lambda/912)^3 \quad (7)$$

and

$$\sigma_{He II}(\lambda) = 16 \sigma_0 g_{He II}(\lambda) (\lambda/912)^3, \quad (8)$$

where  $\sigma_0 = 7.91 \times 10^{-18}$  cm<sup>2</sup>. The hydrogen Gaunt factors  $g_H(\lambda)$  were tabulated by Karzas & Latter (1961), and the He II Gaunt factor is given by  $g_{He II}(\lambda) = g_H(4\lambda)$ . For the cross sections of neutral helium tabulated by West & Marr (1976), Rumph et al. (1994) give the following polynomial fit

$$\log_{10} \sigma_{He I}(\lambda) = \sum_{i=0}^7 c_i (\log_{10} \lambda)^i, \quad (9)$$

where the coefficients  $c_i$  are summarized in Table 1. This expression gives the mean values for  $\sigma_{He I}(\lambda)$ . However, as shown in Figure 1 of Rumph et al. (1994), there exist three autoionizing resonances between 190 and 196 Å that can influence the continuum absorption in the EIT and *TRACE* channels around 195 Å. The real effect depends on the actual shape and intensity of the Fe XII lines that fall into the 195 Å channel. Since we do not make any quantitative data analysis in this paper, we do not further consider these resonances, postponing their study to another paper.

The above representation gives all cross sections in a simple analytical form, where only the Gaunt factors have to be taken from a table. Therefore, this approach can be directly used for any EUV line that lies below 912 Å. Since the Gaunt factors always lie in the range between 0.8 and 1.0 for all wavelengths

TABLE 2  
VALUES FOR GAUNT FACTORS AND ABSORPTION CROSS SECTIONS

$\lambda$ (Å)	$E$ (ryd)	$g_H$	$g_{He II}$	$\sigma_H$ (cm <sup>2</sup> )	$\sigma_{He I}$ (cm <sup>2</sup> )	$\sigma_{He II}$ (cm <sup>2</sup> )
171.....	5.3	0.99	0.86	$5.16 \times 10^{-20}$	$9.25 \times 10^{-19}$	$7.17 \times 10^{-19}$
195.....	4.7	0.99	0.83	$7.65 \times 10^{-20}$	$1.22 \times 10^{-18}$	$1.03 \times 10^{-18}$
284.....	3.2	0.99	...	$2.36 \times 10^{-19}$	$2.58 \times 10^{-18}$	...
912.....	1.0	0.80	...	$6.33 \times 10^{-18}$	...	...

under consideration, one could neglect them and use an approximation  $g \approx 1$ . In this paper, however, we use the exact values to obtain better accuracy. The absorption properties are summarized in Table 2, where  $E$  is the photon energy in rydbergs,  $g_H$  and  $g_{He II}$  are the Gaunt factors for hydrogen and helium, and  $\sigma_H$ ,  $\sigma_{He I}$ , and  $\sigma_{He II}$  are the absorption cross sections.

As a next step we normalize all optical-thickness values to the one obtained for the hydrogen Lyman continuum head, which is given by

$$\tau_{912} = N_H(1 - i)\sigma_H(912). \quad (10)$$

With this relation we obtain the ratio

$$\tau/\tau_{912} = \frac{\sigma_H}{\sigma_H(912)} + \frac{r_{He}}{1 - i} \left[ (1 - j_1 - j_2) \frac{\sigma_{He I}}{\sigma_H(912)} + j_1 \frac{\sigma_{He II}}{\sigma_H(912)} \right]. \quad (11)$$

This equation allows us to calculate optical-thickness ratios for any set of values of  $r_{He}$ ,  $i$ ,  $j_1$ , and  $j_2$ . The value  $\tau_{912}$  can be determined, e.g., from correlations given in our Figure 2.

#### 4.2. Numerical Results

To compute the opacity ratios given by equation (11), one needs to know the actual ionization degrees  $i$ ,  $j_1$ , and  $j_2$ . How-

ever, under typical prominence/filament conditions, these degrees are far from being purely dependent on plasma temperature. The reason is that prominences are not in an LTE state, and their excitation and ionization equilibrium is determined to a large extent by strong radiation coming from the solar disk. In such a situation one has to solve a rather complex non-LTE problem of radiative transfer and statistical equilibrium for hydrogen and helium line and continuum transitions. In the case of hydrogen this was done for prominences and filaments as discussed in § 2. In Figure 3 we show the hydrogen ionization degree  $i$  corresponding to filament models used in Figure 2. From this figure we can see that higher  $i$  at low temperatures can be achieved only for small opacities when the incident radiation can penetrate into the slab. By increasing the temperature,  $i$  is also increased and becomes less dependent on the opacity. The statistical equilibrium for helium was recently studied by Labrosse & Gouttebroze (2001, 2004). N. Labrosse (2004, private communication) has also shown that while  $j_2$  is very low under most prominence conditions,  $j_1$  can at the same time vary from small values up to about 0.95. For cool structures these values for  $j_1$  are due to ionization by incident solar radiation and to a lesser extent due to temperature effects.

For our illustrative computations we take as representative values  $r_{He} = 0.1$ ,  $i = 0.5$  and put  $j_2 = 0$ . In order to test the sensitivity of our results to the first helium ionization, we select two values,  $j_1 = 0$  and  $j_1 = 0.3$ . The results for these calculations are given in Table 3. From this table one sees that the optical thickness in the lines at 171 and 195 Å is rather insensitive to the actual first-ionization degree of helium; and even for  $\lambda = 284$  Å the values differ only by 20% (although in the extreme case of  $j_1 \rightarrow 1$  this difference can become quite large, and the resulting  $\tau$  could be decreased by factors of 2–3).

Our finding that the opacity at wavelengths 171 and 195 Å practically does not depend on the first-ionization degree of helium can be easily understood by inspecting Table 2. We see that  $\sigma_{He I}$  differs from  $\sigma_{He II}$  only by 20%–30% and, therefore, assuming an equality between these two cross sections the terms containing  $j_1$  in equation (11) cancel (note that this approximation was already used by Mein et al. [2001] in their quantitative analysis of TRACE data). For the opacity ratios we then get the following simple formulae (with the data from Table 2):

$$\tau_{171}/\tau_{912} \simeq 8.15 \times 10^{-3} + 1.46 \times 10^{-2} f(i) \quad (12)$$

TABLE 3  
RATIOS OF OPTICAL THICKNESSES

$\lambda$ (Å)	$\tau/\tau_{912}$ ( $j_1 = 0.0$ )	$\tau/\tau_{912}$ ( $j_1 = 0.3$ )
171.....	$3.74 \times 10^{-2}$	$3.54 \times 10^{-2}$
195.....	$5.06 \times 10^{-2}$	$4.88 \times 10^{-2}$
284.....	$1.19 \times 10^{-1}$	$9.43 \times 10^{-2}$

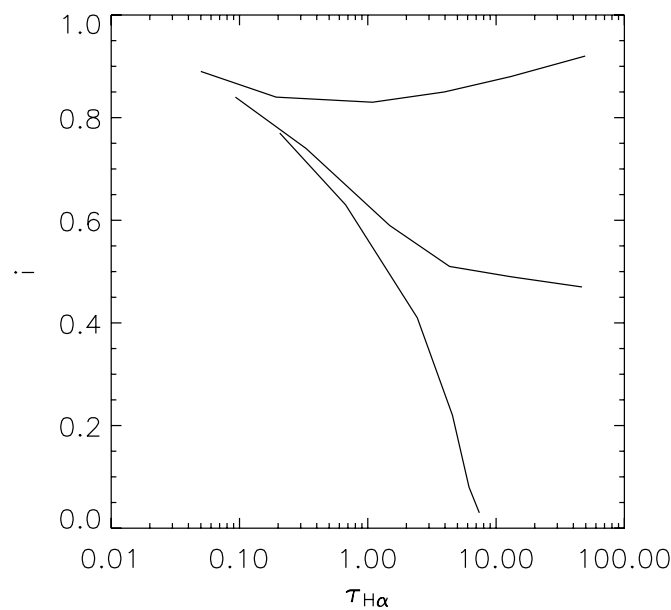


FIG. 3.—Hydrogen ionization degree  $i$  at the center of the one-dimensional filament slab. The same models as in Fig. 1 are used. The three curves correspond (bottom to top) to three filament temperatures  $T = 6000, 8000,$  and  $10,000$  K. For  $T = 15,000$  K the ionization degree reaches approximately unity.

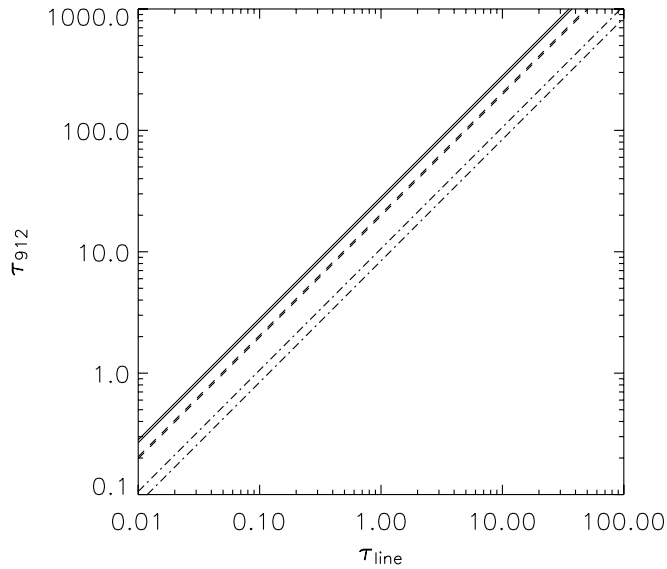


FIG. 4.—Correlation of continuum optical thickness at the wavelength position of different iron lines and at the Lyman continuum at 912 Å. *Solid lines*:  $\lambda = 171$  Å; *dashed lines*:  $\lambda = 195$  Å; and *dot-dashed lines*:  $\lambda = 284$  Å. Lower lines correspond to  $j_1 = 0.0$  and upper lines to  $j_1 = 0.3$ .

and

$$\tau_{195}/\tau_{912} \simeq 12.09 \times 10^{-3} + 1.93 \times 10^{-2} f(i). \quad (13)$$

Here we have again used  $r_{\text{He}} = 0.1$  and put  $j_2 = 0$ . The great advantage of these formulae is that they no longer depend on the first-ionization degree of helium. However, the function

$$f(i) = \frac{1}{1-i} \quad (14)$$

still depends on the hydrogen ionization degree.

We now want to compare the values of these optical thicknesses with the ones derived for the  $\text{H}\alpha$  line of hydrogen by using the isothermal–isobaric slab models. For this purpose we have constructed a plot that gives the continuum optical thickness at  $\lambda = 912$  Å as a function of the continuum optical thickness at the position of the iron lines considered. The results are shown in Figure 4. From this figure one finds that both the lines for  $\tau_{171}$  and those for  $\tau_{195}$  are very close to the curves for  $\tau_{\text{H}\alpha}$  that were calculated for  $T = 6000$ – $8000$  K. The lines obtained for  $\tau_{284}$  are somewhat below the  $\tau_{\text{H}\alpha}$  curves. From these comparisons we conclude that at the positions of all three iron lines the continuum has, at least in terms of orders of magnitude, the same absorption properties as the  $\text{H}\alpha$  line. For higher temperatures the continuum absorption is even weaker. An immediate and extremely important consequence of this result is that the dark structures seen by EIT or *TRACE* in iron lines cannot be due to absorption by resonance continua unless we can clearly identify their  $\text{H}\alpha$  counterparts. Therefore, another mechanism of EUV darkening has to be considered, namely volume blocking, which is discussed in the next section.

### 5. BLOCKING OF CORONAL LINE RADIATION

We assume that the corona is spherically symmetric and its line emissivity is given by

$$\epsilon = \epsilon_0 e^{-h/H}, \quad (15)$$

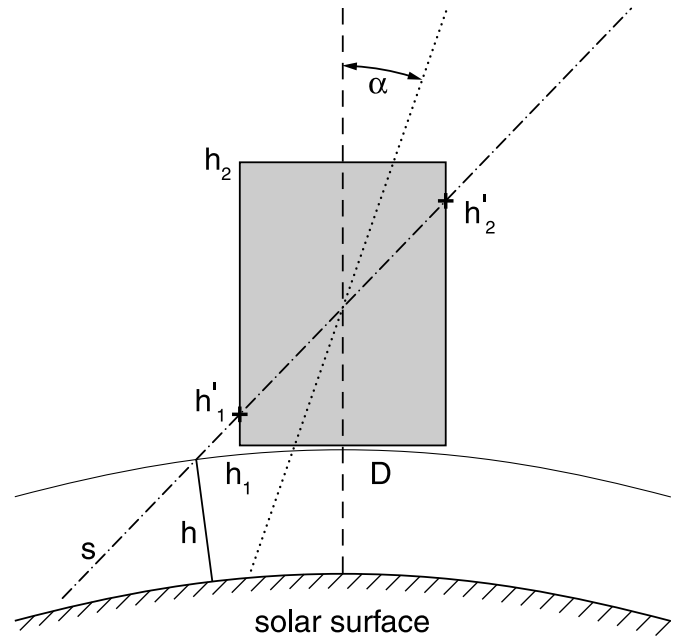


FIG. 5.—Sketch of the filament geometry considered. The filament extends in height from  $h_1$  to  $h_2$  and has a width of  $D$ . Three different types of line of sight are drawn. *Dashed line*: view directly from the top ( $\alpha = 0$ ); *dotted line*: filament seen at small viewing angle  $\alpha$ ; *dot-dashed line*: large viewing angle  $\alpha$  (in this case the cool region extends only from  $h'_1$  to  $h'_2$ ). Also shown are a surface of constant emissivity (*thin line*) at a height  $h$  and the line-of-sight coordinate  $s$ .

where  $h$  is the height above the solar surface and  $H$  the scale height of the emissivity. We further denote by  $L$  the length along the line of sight of any cool structure under consideration. For those structures that are close to the disk center one finds for the total intensity  $I_0$  the relation

$$I_0 = \int_0^\infty \epsilon_0 e^{-h/H} dh, \quad (16)$$

and the intensity corresponding to the amount of blocked radiation (due to the lack of coronal emission in a given volume) is given by

$$I_b = \int_{h_1}^{h_2} \epsilon_0 e^{-h/H} dh. \quad (17)$$

For the details of the geometry considered here, see Figure 5.

If we further assume  $h_1 = 0$  and  $h_2 = L$ , we get

$$I_b = H\epsilon_0 \left(1 - e^{-L/H}\right), \quad (18)$$

as well as

$$I_0 = H\epsilon_0. \quad (19)$$

This leads to a *blocking contrast ratio*

$$r_b = e^{-L/H}, \quad (20)$$

where  $r_b$  is defined as

$$r_b = \frac{I_0 - I_b}{I_0}. \quad (21)$$

If the filament is not very far from the disk center one can use the plane parallel approximation. In a spherical atmosphere equation (17) has to be replaced by the expression

$$I_b = \int_{s_1}^{s_2} \epsilon_0 e^{-h/H} ds, \quad (22)$$

with  $s$  given by

$$s = \sqrt{(R_\odot \cos \alpha)^2 + 2R_\odot h + h^2} - R_\odot \cos \alpha, \quad (23)$$

where  $\alpha$  denotes the position angle of the structure as measured from the disk center and  $s$  represents the coordinate along the line of sight. Assuming now that  $h \leq H$  holds (because this is the region of major contribution to the integral in eq. [22]), we find that for  $\alpha < \alpha_{\text{cr}}$  one obtains the relation

$$s \approx \frac{h}{\cos \alpha}, \quad (24)$$

and the critical value of  $\alpha$  is given by

$$\cos \alpha_{\text{cr}} = \sqrt{\frac{2H}{R_\odot}}. \quad (25)$$

Equation (24), together with integral of equation (22), now represents the plane parallel approximation. For  $H = 0.1R_\odot$  one obtains  $\alpha_{\text{cr}} \approx 63^\circ$ . In the plane parallel approximation one then has to replace the scale height  $H$  by the scale height measured along the line of sight, which is given by

$$H' = H / \cos \alpha. \quad (26)$$

With this modification one can then still use our equations (18) and (19).

No simple relations can be used for filament positions between  $\alpha_{\text{cr}}$  and the solar limb, where the curvature of the atmosphere has to be included. But for the total intensity one has to demand that it go smoothly from that of the plane parallel approximation to one-half of the value, which we calculate for the corona just above the limb.

The situation is more complicated for structures observed above the solar limb. There the appropriate line-of-sight variation of  $\epsilon$  has to be used in the integration (for relevant formulas, see the Appendix in Heinzel et al. [2003]). The general case cannot be calculated analytically, but for all cases with  $H \ll R_\odot$  an approximate solution can be derived. For the line of sight passing close to the solar limb one arrives at

$$I_0 \approx \epsilon_0 \sqrt{2\pi R_\odot H}. \quad (27)$$

This equation indicates that the main contribution to the intensity originates from a region along the line of sight amounting to  $(2\pi R_\odot H)^{1/2}$ . With  $H = 40,000$  km this length is 420,000 km. This length also determines the degree of concentration of the radiation towards the plane of the sky. As long as the condition  $L < (2\pi R_\odot H)^{1/2}$  holds, one finds for the intensity of the blocked radiation an estimate

$$I_b \approx L\epsilon_0. \quad (28)$$

With this estimate one arrives at

$$r_b \approx 1 - L / \sqrt{2\pi R_\odot H} \quad (29)$$

or

$$r_b \approx 1 - L / (420,000), \quad (30)$$

where  $L$  has to be taken in kilometers. Note that equation (29) is valid irrespective of the height at which the line of sight passes. The value  $\epsilon_0$  in equations (27) and (28) is in general replaced by the height-dependent  $\epsilon$ , but it cancels in our definition of  $r_b$ .

Our equations (18) and (20) show that for disk observations a blocking length of  $(0.2-0.5)H$  can already give a strong blocking signal. But on the limb the blocking length must be much larger (typically around  $10^5$  km) to give a similar contrast. This behavior is due to the fact that the coronal emission is much more extended tangentially to the solar surface than in the radial direction. This property is also reflected by the fact that the total intensity is much lower at disk center than above the solar limb. The ratio of these intensities is given by

$$\frac{I_0^{\text{disk}}}{I_0^{\text{limb}}} = \frac{1}{\sqrt{2\pi R_\odot / H}}. \quad (31)$$

This leads to an intensity ratio of about 1/10 for the case of  $H = 40,000$  km. However, when one approaches the solar limb the corresponding intensity ratio always goes to the value of 1/2.

There are also some coronal lines that lie above the Lyman continuum head of hydrogen and that therefore are not affected by hydrogen absorption. An example of a coronal line above the Lyman continuum head is the Fe XII line at 1242 Å, which is observed by SOHO/SUMER. This then means that observations in such lines can be used in the future to find a clear distinction between the effects of blocking and of absorption.

## 6. PROMINENCES ON THE LIMB

As we show in the previous sections the continuum optical thickness at the wavelength position of the EUV iron lines has a value that is comparable to that of the H $\alpha$  line. This, then, implies that for any prominence on the limb that has a sizeable optical thickness in H $\alpha$  there should also be a measurable absorption in the coronal iron lines. In the case that the extension of the prominence along the line of sight is sufficiently small compared with the coronal scale height of the line under consideration, and if the corona is symmetrical along the line of sight with respect to the prominence position, one finds that one-half of the total radiation comes from behind the prominence (this background radiation is partially absorbed), and the other half comes from the foreground. In such a situation the observed intensity should amount to

$$I = \frac{1}{2} I_0 (1 + e^{-\tau}), \quad (32)$$

where  $I_0$  is the total coronal intensity as given by equation (27), and  $\tau$  the value of the optical thickness at the wavelength of the iron line. The contrast with respect to the quiet Sun is then given by the relation

$$r = \frac{1}{2} (1 + e^{-\tau}). \quad (33)$$

This means that the maximum possible contrast is  $r = \frac{1}{2}$  for the case in which  $\tau$  becomes large.

The values of  $\tau$  for the three iron lines can thus be inferred from the observed contrasts. Then one can determine  $\tau_{912}$  by using equation (11) and see whether this determination is unique for all lines. If so, this will give strong support for the simple model considered here. Finally,  $\tau_{H\alpha}$  can be estimated from the correlation plots in Figure 2. However, such an idealized situation is probably not very common because both assumptions made above are rather restrictive.

The extension along the line of sight can be large for the following reasons:

1. Although the prominence sheet is thin it might be observed at a very small viewing angle (edge-on). Then the projection effect can become very large.

2. There is also the possibility that extended cool regions exist around the prominence (so-called ‘‘EUV extensions’’), which is discussed below.

This effect will lead to substantial volume blocking that depends on the coronal scale height for the line under consideration. We can generalize equation (33) to account for the volume-blocking effect, and we get

$$r = \frac{1}{2}(1 + e^{-\tau})r_b. \quad (34)$$

The limiting cases are  $r = r_b$  (with  $r_b$  given by eq. [29]) for negligible  $\tau$  and  $r = \frac{1}{2}r_b$  for large  $\tau$ . By including this blocking effect into spectral diagnostics one should arrive at better fits to the observations.

There is also the problem that the corona often shows strong irregularities. Such inhomogeneities can cause two types of difficulties for the modeling. First, there is no longer a well-defined value of the intensity  $I_0$ , which is needed for equation (32). Therefore, this equation will not give reliable results in this case. Second, the assumed symmetry between foreground and background can also break down. This will also enter into equation (32). Under such circumstances the results obtained by our model have to be considered rough approximations with possible large uncertainties.

## 7. FILAMENTS ON THE DISK

Filaments on the disk are the same structures as prominences on the limb. The effects that these cool filaments have on the coronal lines are identical to those that are present on the limb. The differences arise only from the geometrical configuration. The absorption only acts on that part of the radiation that is emitted from underneath the filament. Since filaments in general reach down to low coronal heights, a rather small amount of radiation originates from below the filament. Note that this behavior is quite different from that seen in transition region lines. In addition, filaments are usually very extended in height. Therefore, as long as one looks down in an approximately radial direction, a large fraction of the coronal radiation is blocked. Under these circumstances absorption plays a less dominant role than in the case of limb prominences.

Here we follow the modeling of Heinzel et al. (2003) and Schwartz et al. (2004). As in the previous section we assume a spherically symmetric exponentially decaying coronal emission distribution.

For filaments observed away from the disk center there is always some projection effect. If we denote the angle between the radial direction and the line of sight by  $\alpha$  (which is identical to the position angle used in § 5; see also Fig. 5 for geom-

etry), then the coordinate measured along the line of sight is given by

$$h' = h / \cos \alpha. \quad (35)$$

We also denote by  $h_1$  the height of the bottom of the prominence and by  $h_2$  that of its top (see Fig. 5). Here the heights are measured in a vertical direction, whereas the length  $L$  considered in § 5 is along the line of sight. Then the total filament intensity can be easily calculated as

$$I_{\text{fil}} = \epsilon_0 \frac{H}{\cos \alpha} \left[ \left(1 - e^{-h_1/H}\right) e^{-\tau} + e^{-h_2/H} \right], \quad (36)$$

and for the quiet-Sun intensity one has

$$I_0 = \epsilon_0 \frac{H}{\cos \alpha}. \quad (37)$$

This leads to a contrast ratio

$$r = \left(1 - e^{-h_1/H}\right) e^{-\tau} + e^{-h_2/H}. \quad (38)$$

This equation holds for all the lines considered in this paper, where  $\tau$  for each of these lines is taken according to our Figure 4. If we now measure the contrast  $r$  for all lines and can independently determine the scale heights  $H$  of the different lines, we end up with three equations for the three unknowns,  $\tau_{912}$ ,  $h_1$ , and  $h_2$ . This procedure therefore allows us to calculate the geometry and the optical thickness of the filament.

This simple consideration holds only in the case of

$$\tan \alpha < \frac{D}{h_2 - h_1}, \quad (39)$$

where  $D$  is the width of the prominence sheet. This constraint then implies that if the prominence is narrow (compared with its height), only very small values of the viewing angle are allowed. But if this condition is not fulfilled, then the line of sight will cut through the two sides of the prominence. Under these circumstances one has to interpret  $h_1$  as the height of the lower cutting point and  $h_2$  as that of the upper one. With this modification equation (38) can still be used. In this case one finds

$$D = (h_2 - h_1) \tan \alpha. \quad (40)$$

As in the case of the limb prominences described in the previous section, the main source of uncertainty arises from the assumption of a uniformly exponential corona as described in equation (15). Therefore, one also has to be cautious with the results calculated for disk configurations. But within these limitations the procedure should give us some general idea about the filament geometry (see Schwartz et al. 2004).

## 8. PRESENCE OF EXTENDED EUV STRUCTURES

Using *SOHO*/CDS observations Heinzel et al. (2001) and Schmieder et al. (2003) found dark structures that are much more extended than the corresponding  $H\alpha$  filament. The particular EUV lines that they used are Si XII at 520.60 Å, Ca X at 557.77 Å, Ne VI at 572.80 Å, Mg X at 624.94 Å, and O V at 629.73 Å. Schwartz et al. (2004) modeled these structures as extended cool regions around the  $H\alpha$  filament. From the observed intensities of EUV lines they calculated the geometry of the structures. They found that their heights are comparable to

those of the associated  $H\alpha$  filaments, but their horizontal extension is much larger. Since the EUV filament extensions are not visible in  $H\alpha$ , one must conclude that they also have a negligible optical thickness in the EIT and *TRACE* iron lines, as we have demonstrated in our Figure 4. This is why EUV prominence extensions were not detected on off-limb EIT or *TRACE* images. Nevertheless, they may contribute to the blocking of these lines. We now describe the effects of these extended cool regions that are not visible in the  $H\alpha$  line on the contrast of iron lines.

For prominences on the limb the situation is rather simple. In this case the blocking takes away some radiation along the line of sight characterized by its path length  $L$ , and the corresponding  $r_b$  can be computed from equation (29). But unless  $L$  is very large (of the order of  $10^5$  km or larger), the contrast of EUV prominence extensions seen on the limb is quite small compared with that of the  $H\alpha$  counterparts.

Concerning the disk observations the situation is similar, but now one has to use our equation (38) to calculate the contrast ratio. With  $\tau \ll 1$  we get

$$r_b = 1 - e^{-h_1/H} + e^{-h_2/H}. \quad (41)$$

Contrary to prominences on the limb, the EUV filament extensions can be seen in iron lines rather easily, as long as their height extension is comparable to or larger than the scale height  $H$  for the given line. The importance of the volume blocking in *TRACE* iron lines was already demonstrated in Schmieder et al. (2004).

## 9. CONCLUSIONS

In this paper we studied the behavior of dark structures seen in coronal channels of *SOHO*/EIT and *TRACE* centered around the iron lines at 171, 195, and 284 Å. These features are supposed to correspond to cool prominence-like structures, and they produce the brightness reduction of coronal iron lines because of the absorption by resonance hydrogen and helium continua and because of volume blocking. We computed the correlations between the continuum opacity at the wavelength position of iron lines and that at the hydrogen Lyman continuum head. Moreover, using the non-LTE radiative-transfer technique, we derived the relation between the hydrogen Lyman continuum opacity and the opacity of the hydrogen  $H\alpha$  line. These relations then allowed us to discuss the visibility (contrast) of limb prominences, as well as disk filaments, as seen by both EIT and *TRACE*. Our

main conclusion is that the structures for which one can identify their  $H\alpha$  counterparts are due to both the absorption and volume blocking, and the relative importance of these two mechanisms depends on the  $H\alpha$  opacity, on the temperature, and the geometrical extension of the structure along the line of sight. On the other hand, those dark structures that have no visible  $H\alpha$  counterpart have optically thin resonance continua at the wavelength positions of iron lines, and thus the absorption mechanism plays a negligible role. Their darkness is then entirely due to volume blocking. Note, however, that dark *loop structures* projected onto the disk must be entirely due to absorption because they are geometrically too thin to block efficiently the coronal radiation. That their visibility therefore results only from absorption implies a rather high column density, and they should also be visible in the  $H\alpha$  line.

In the paper we give several useful relations and tables that can be used in interpreting the EIT and *TRACE* data. However, there is still an uncertainty in the ionization degree of hydrogen and helium. Since this is strongly model dependent, one would need more detailed non-LTE calculations for the particular cases investigated. Such modeling is now in progress for a hydrogen-helium plasma under typical prominence-like conditions.

We also briefly discuss the visibility of the so-called EUV filament extensions recently discovered from *SOHO*/CDS observations. Since these extensions, by definition, have no  $H\alpha$  counterparts, according to the results of this paper they should not produce any significant absorption of coronal iron line radiation at the wavelengths considered here. Therefore, when they are visible on EIT or *TRACE* images, their visibility must be interpreted as volume blocking.

Finally, we want to stress that our formulation describing the absorption and volume blocking is quite general and can be equally well used in analyzing other EUV line observations taken, for example, by the *SOHO* CDS or SUMER instruments. In this respect equations (34) and (38) are of a particular interest for prominence and filament observations, respectively.

This work was supported by grant A3003203 from the Academy of Sciences of the Czech Republic. U. A. thanks the Astronomical Institute in Ondřejov for support. We also thank the referee for his useful comments. *SOHO* is a space mission based on international cooperation between ESA and NASA.

## REFERENCES

- Anzer, U., & Heinzel, P. 1999, *A&A*, 349, 974  
 Chiuderi Drago, F., Alissandrakis, C. E., Bastian, T., Bocchialini, K., & Harrison, R. A. 2001, *Sol. Phys.*, 199, 115  
 Engvold, O., Jakobsson, H., Tandberg-Hanssen, E., Gurman, J. B., & Moses, D. 2001, *Sol. Phys.*, 202, 293  
 Gouttebroze, P., Heinzel, P., & Vial, J.-C. 1993, *A&AS*, 99, 513  
 Heinzel, P., Anzer, U., & Schmieder, B. 2003, *Sol. Phys.*, 216, 159  
 Heinzel, P., Gouttebroze, P., & Vial, J.-C. 1994, *A&A*, 292, 656  
 Heinzel, P., Schmieder, B., & Tziotziou, K. 2001, *ApJ*, 561, L223  
 Heinzel, P., Schmieder, B., & Vial, J.-C. 1997, in *Proc. Fifth SOHO Workshop*, ed. A. Wilson (ESA SP-404; Noordwijk: ESA), 427  
 Karzas, W. J., & Latter, R. 1961, *ApJS*, 6, 167  
 Kucera, T., Andretta, V., & Poland, A. I. 1998, *Sol. Phys.*, 183, 107  
 Labrosse, N., & Gouttebroze, P. 2001, *A&A*, 380, 323  
 ———. 2004, *ApJ*, 617, 614  
 Mein, N., Schmieder, B., DeLuca, E. E., Heinzel, P., Mein, P., Malherbe, J.-M., & Staiger, J. 2001, *ApJ*, 556, 438  
 Mihalas, D. 1978, *Stellar Atmospheres* (2nd ed.; San Francisco: Freeman)  
 Rumph, T., Bowyer, S., & Vennes, S. 1994, *AJ*, 107, 2108  
 Schmal, E. J., & Orrall, F. Q. 1979, *ApJ*, 231, L41  
 Schmieder, B., Lin, Y., Heinzel, P., & Schwartz, P. 2004, *Sol. Phys.*, 221, 297  
 Schmieder, B., Tziotziou, K., & Heinzel, P. 2003, *A&A*, 401, 361  
 Schwartz, P., Heinzel, P., Anzer, U., & Schmieder, B. 2004, *A&A*, 421, 323  
 West, J. B., & Marr, G. V. 1976, *Proc. R. Soc. London A*, 349, 397